UNIVERSITY OF STRASBOURG

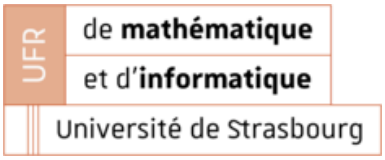

CSMI : Scientific Computing and Mathematics of Innovation

The Study of The N-Links Swimmer for Monoflagellate Micro-swimmers

Supervisors:
Lucas Palazzolo
Laetitia Giraldi

Author:
Komi Joseph Béni ASSIGBE

Contents

Acknowledgement

I would like to express my deepest gratitude to my internship supervisor, Mrs Laetitia Giraldi, and Mr. Lucas Palazzolo, for their invaluable guidance and support throughout this internship. Their expertise and encouragement were essential in helping me navigate through this experience.

I am also profoundly thankful to Mr. Christophe Prud'homme for his assistance in securing this internship and his insightful counsel throughout the entire semester. His support was crucial in the initial stages and continued to be invaluable as the internship progressed.

I am truly grateful for the opportunity to work on such exciting topics that encompass mathematical modeling and informatics. I would like to extend my heartfelt thanks to my main supervisor for his patience, meekness, and unwavering guidance, which were instrumental in overcoming the challenges I faced during this internship. His remarkable ability to simplify and explain even the most complex concepts is a true gift.

This experience has been incredibly enriching, and I am sincerely appreciative of everyone who contributed to its success.

Chapter 1

Introduction

Microrobotics is a field with diverse applications, such as environmental monitoring, medical procedures, and micro-assembly. Designing microrobots that can efficiently swim in fluids is challenging due to the dominance of viscosity over inertia at the microscale. Researchers have looked to biological microorganisms like bacteria and sperm cells, which have evolved effective swimming mechanisms for low-Reynolds number. Most microrobots rely on remote power sources, as implementing onboard energy sources at this scale is difficult. One of the pioneering works in this field taylor [11] who established the mathematical settings for the problem of biological self-propulsion powered by thin undilating filaments.

1.1 Swimming in Micro-scale

The general equations govering fluid dynamics are the Navier-Stokes equations, which in the case of incompressible Newtonian fluid are given by:

$$\begin{aligned} \rho\left(\frac{\partial v}{\partial t} + v \cdot \nabla v\right) &= -\nabla p + \mu \nabla^2 v + \rho g, \\ \nabla \cdot v &= 0. \end{aligned} \tag{1.1}$$

where ρ is the fluid density, v is the fluid velocity, p is the fluid pressure, μ is the dynamic viscosity, and g is the gravitational acceleration. The Navier-stokes equations can be non-dimensionalized by introducing dimensionless variables.

Let us consider some characteric variables : L the characteristic length scale, U the characteristic velocity scale, P the characteristic pressure scale, T the characteristic time scale.

Let's define the dimensionless variables as follows: $\tilde{t} = \frac{t}{T}$, $\tilde{x} = \frac{x}{L}$, $\tilde{v} = \frac{v}{U}$, $\tilde{p} = \frac{p}{P}$ that leads to the dimensionless form of the Navier-Stokes equations according to Pozrikidis and Jankowski in [9] :

$$\begin{aligned} \beta\frac{\partial\tilde{v}}{\partial\tilde{t}} + Re\,\tilde{v}\cdot\nabla\tilde{v} = -\nabla\tilde{p} + \nabla^2\tilde{v} + \frac{Re}{Fr^2}\frac{g}{|g|}, \\ \nabla\cdot\tilde{v} = 0. \end{aligned} \tag{1.2}$$

where $\beta = \frac{\rho UL^2}{\mu T}$ is a frequency parameter that express the relative magnitudes of the inertial acceleration force and the viscous force, $Re = \frac{\rho UL}{\nu}$ is the Reynolds number, $Fr = \frac{U}{\sqrt{gL}}$ is the Froude number.

1.2 Reynolds number

The Reynolds number describes the transport properties of a fluid or a particle moving in a fluid. At the macroscopic scale, the Reynolds number is high, which means that inertial forces are dominant over viscous forces. For example, for humans or organisms such as fish swimming in water, the Reynolds number is in the range of 10^4. For micro-organisms such as bacteria or sperm cells, the Reynolds number is in the range of 10^{-2} to 10^4.

At low Reynolds number, any movement is reversible, if an organism (like a micro-swimmer) attempts to move forward by changing its shape and then tries to reverse that movement by returning to its original shape, the backward movement will exactly cancel out the forward movement. As a result, the organism doesn't make any net progress in its motion; the forces involved are dominated by viscosity rather than inertia. Due to the low Reynolds number, the equations governing the movement, known as the **Stokes equations**, can be expressed as follows :

$$\begin{aligned} \mu\nabla^2 v - \nabla p = 0, \\ \nabla\cdot v = 0. \end{aligned} \tag{1.3}$$

The time irreversibility condition is famously known as Purcell's scallop theorem, [10], named after that a scallop cannot generate a non zero net displacement at low Reynold number by a reciprocal motion.

In nature, the micro-organism like bacteria such as *Escherichia coli* propel itself by rotating their flagella, which creates traveling helical waves, and also single flagellated eukaryotic cells like sperm cells swim by beating their flagellum in a helical motion, also ciliates such as *Opalina* swim by non-reciprocal shape deformations resulting from the asymmetrical beating of their cilia.

There are various methods of propulsion at the micro-scale, each suited to different organisms and environments. Ciliary beating is one such method, where coordinated wave-like motions of cilia propel the organism through its environment. Another method is flagellar beating, which involves the rotation or whipping motion of one or more flagella to generate thrust. Additionally, some organisms use a corkscrew-type rotating propulsion, where the body rotates in a helical manner to move forward, As illustrated in Figure 1.2

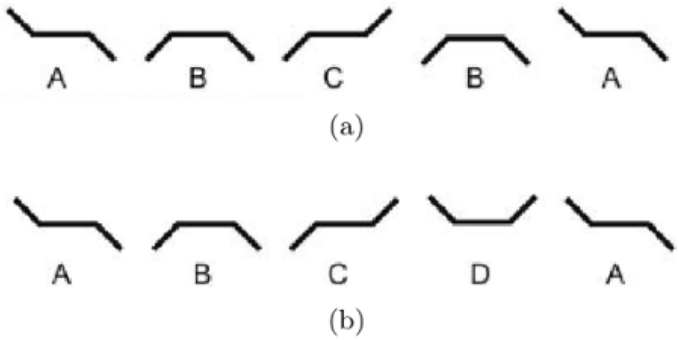

Figure 1.1: Example of 3-Links of Purcell [10] (a) Reciprocal motion and (b) Non-reciprocal motion

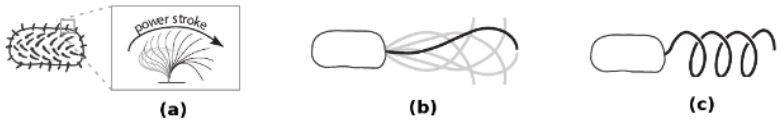

Figure 1.2: (a) : Locomotion methods at Micro-scale [1] : Propulsion by cilliary beating, (b):Propulsion by flagellar beating, (c) : Corkscrew-type rotating propulsion

1.3 Internship Objectifs

"During this internship, I studied the 3D N-links model of micro-swimmers based on the thesis [2] and worked on validating the model using an already provided code. The validation was carried out in two stages: first, by studying planar motion [4], and then by examining non-planar motion [7], comparing the obtained results with those presented in the referenced articles, and conducting numerical simulations to analyze the factors influencing the micro-swimmer's movement. Subsequently, I focused on the optimal control of flagellar displacement, which involves determining the most effective

strategies to maximize or optimize the movement of the micro-swimmer. For the tools, i used in this internship, i used

- Python as Programming Language and his library as Numpy, Casadi, scipy
- Github
- Slack for Communication

Chapter 2

N-Links Modelisation

2.1 Introduction

The modelisation of a micro-swimmer motion in a fluid is quite challenging things, due to the coupled interaction between the fluid and the body, and between the body and the fluid, as well as the elasticity of the tail. In this study, we specifically focus on mono-flagellated micro-swimmers. A full description of the dynamics of the swimmer would require the resolution of a system of coupled partial differential equations that is too costly to be used in an optimization process.

Hence, the main difficulty of developing the model was the trade-off between its accuracy, as it needs to reliably predict the displacements of the experimental swimmer, and its numerical complexity, as it needs to be computationally inexpensive enough to be used to numerically solve the optimal control problem.

We used a simplified apporach to modeling the swimmer, where the hydrodyammic effects are simplified by using a local drag approximation resistive force theory (RFT), and where the shape of the tail is discretized into an articulated chain of N slender rods, generalizing the planar swimmer models of Moreau et al. 2018, Alouges et al. 2013 in [8]

Using these simplifications, the dynamics of the swimmer are formulated as an ODE system that can be easily assembled and solved, providing a valuable tool for the quantitative description of the motion of biological mono-flagellated micro-swimmers.

2.2 The Resistive Force Theory approximation

The RFT was introduced by Gray and Hannock [6] to model the hydrodynamics of slender bodies moving in a viscous fluid at low Reynolds number. The aim is to approximate the hydrodynamic forces on a slender filament at low Reynolds number by neglecting the interactions on the global scale in favor of the local anisotropic friction of the surface of the slender body with the nearby fluid.

The main thing about this theory is that, at low Reynolds number and for every slend filament, we can established a linear relationship between the viscous drag density on an infinitesimal segment of the filament and the local velocity of the fluid at that point. From this, we are able to compute the viscous forces and torques on a moving and deforming slender filament by summing the density of forces over the filament.

Let us consider a thin filament immersed in a viscous fluid and examine an infinitesimal segment of the filament at a point $x(s)$ along its arc length s. The velocity $\dot{x}(s)$ can be decomposed into a tangential component $v(s)$, a normal component $w(s)$, and a binormal component $u(s)$:

$$\dot{x}(s) = \dot{x}(s) \cdot v + \dot{x}(s) \cdot w + \dot{x}(s) \cdot u.$$

The RFT states that the hydrodynamics force density $f(s)$ can be approximated as

$$f(s) = k_{\parallel} \dot{x}(s) \cdot v + k_{\perp} \dot{x}(s) \cdot w + k_{\perp} \dot{x}(s) \cdot u,$$

where $k_{\parallel}$, $k_{\perp}$ are the drag coefficients, which are functions of the shape of the filament and the fluid viscosity. Then we will be able to compute the net hydrodynamic forces and torques (around an arbitrary point x_0) on the filament by integrating the force density over the filament :

$$F = \int_0^L f(s) ds, \quad T = \int_0^L (x_i(s) - x_0) \times f(s) ds.$$

2.3 The N-Link swimmer Model

The swimmer model is composed of a spherical head of radius r and a slender tail of length L approximated by an articulated chain formed by N slender rods of length l as shown in Figure 2.1

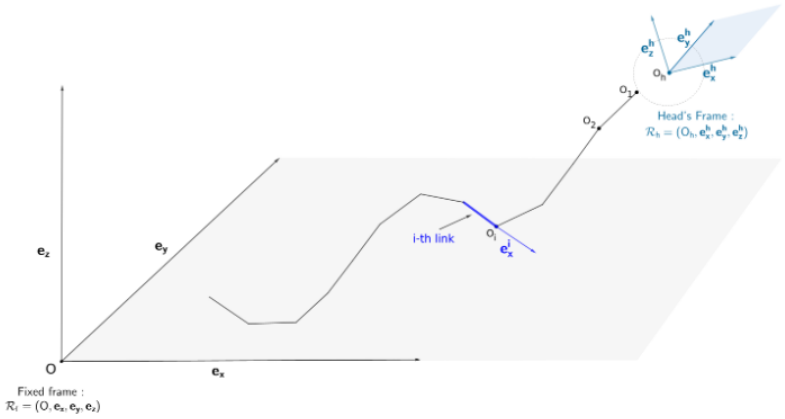

Figure 2.1: The 3D swimmer model features an N-link discretization of the tail [2]. The swimmer's head is oriented relative to a fixed Galilean reference frame. Each link i, is oriented relative to the head frame R_h.

2.3.1 The Kinematics of the swimmer

The Parametrization of the Swimmer

We describe the parametrization of the swimmer's motion from [2]. Let's define X the center of the head and O_1 the point where the first link is attached to the head. We are considering the head moving frame $R_{head} = (X, e_x^h, e_y^h, e_z^h)$ where e_x^h is the unit vector pointing in the direction of the head's long axis, and verifying:

$$O_1 = X - re_x^h \tag{2.1}$$

and unit vector e_y^h and e_z^h are arbitraly chosen to form an orthonormal basis. With r the radius of the head, we compute the coordinate of the i-th link by

$$O_{i+1} = O_i - le_x^i, \quad \forall i \in [1, \ldots, N],$$

where l is the link length, and e_x^i is the unit vector pointing in the direction of the i-th link. According to Figure 2.1, we defined the matrix $R_{\text{head}} \in SO(3)$, by:

$$R_{\text{head}}e_x = e_x^h, \quad R_{\text{head}}e_y = e_y^h, \quad R_{\text{head}}e_z = e_z^h. \tag{2.2}$$

The rotation Matrix is described by the three angles $(\theta_x, \theta_y, \theta_z)$ such as :

$$R_{\text{head}} = R_x(\theta_x)R_y(\theta_y)R_z(\theta_z), \tag{2.3}$$

where R_x, R_y, R_z is the rotation matrix around the x-axis, y-axis, z-axis respectively. and defined for all angle ψ by:

$$R_x(\psi) = \begin{pmatrix} 1 & 0 & 0 \\ 0 & \cos(\psi) & -\sin(\psi) \\ 0 & \sin(\psi) & \cos(\psi) \end{pmatrix},$$

$$R_y(\psi) = \begin{pmatrix} \cos(\psi) & 0 & \sin(\psi) \\ 0 & 1 & 0 \\ -\sin(\psi) & 0 & \cos(\psi) \end{pmatrix}, \tag{2.4}$$

$$R_z(\psi) = \begin{pmatrix} \cos(\psi) & -\sin(\psi) & 0 \\ \sin(\psi) & \cos(\psi) & 0 \\ 0 & 0 & 1 \end{pmatrix}.$$

According to (2.4), the expressions of the position of the i-th link can be expressed as:

$$O_1 = X - rR_{head}e_x,$$

and

$$O_{i+1} = O_i - lR_iR_{head}e_x, \quad \forall i \in [1, \dots N],$$

with R_i the rotation matrix associated to the orientation of the i-th link, defined by

$$R_i = R_y(\phi_y^i)R_z(\phi_z^i),$$

where ϕ_y^i and ϕ_z^i are the angles of the i-th link with respect to the head frame. So, we finally have :

$$O_i = X - rR_{head}e_x - l\sum_{k=1}^{i-1} R_{head}R_ke_x, \quad \forall i \in [1, \dots, N].$$

With these notations, the swimmer can be described by the two sets of variables : The 6 position variables: (X, Θ) where

$$X = (x_h, y_h, z_h) \in \mathbb{R}^3 \quad \text{and}$$

$$\Theta = (\theta_x, \theta_y, \theta_z) \in [0, 2\pi]^3,$$

and the $2N$ shape variables, denoted by

$$\Phi = (\phi_y^1, \phi_z^1, \cdots, \phi_y^N, \phi_z^N).$$

Angular velocity vectors

We introduce the notion of skew-symetric matrices to describe the angular velocity vector. For any skew-symmetric matrix A, there exists a vector $\Omega \in \mathbb{R}^3$ such that for any vector $V \in \mathbb{R}^3$:

$$AV = \Omega \times V, \quad \forall V \in \mathbb{R}^3$$

where A is defined by

$$A = [\Omega]^\times = \begin{bmatrix} 0 & -\Omega_z & \Omega_y \\ \Omega_z & 0 & -\Omega_x \\ -\Omega_y & \Omega_x & 0 \end{bmatrix}.$$

Let's denote by Ω_h the angular velocity vector of the head, and Ω_i the angular velocity vector of the i-th link.

- Ω_h is defined as the cross product associated with the skew-symmetric matrix $\dot{R_{\text{head}}} R_{\text{head}}^T$ and depends linearly on $\dot{\Theta}$ as follows:

$$\Omega_{\text{h}} = L_{\text{head}} \begin{pmatrix} \dot{\theta}_x \\ \dot{\theta}_y \\ \dot{\theta}_z \end{pmatrix}, \tag{2.5}$$

  where

$$L_{\text{head}} = \begin{pmatrix} 1 & 0 & \sin(\theta_y) \\ 0 & \cos(\theta_x) & -\cos(\theta_y)\sin(\theta_x) \\ 0 & \sin(\theta_x) & \cos(\theta_x)\cos(\theta_y) \end{pmatrix}.$$

- Ω_i is defined as the cross product associated with the skew-symmetric matrix $\dot{R}_i {R_i}^T$ and depends linearly on $\begin{pmatrix} \dot{\phi}_x^i \\ \dot{\phi}_y^i \end{pmatrix}$ as follows:

$$\Omega_i = L_i \begin{pmatrix} \dot{\phi}_y^i \\ \dot{\phi}_z^i \end{pmatrix}, \tag{2.6}$$

  where

$$L_i = \begin{pmatrix} 0 & \sin(\phi_y^i) \\ 1 & 0 \\ 0 & \cos(\phi_y^i) \end{pmatrix}.$$

Forces and torques on the head of the swimmer

The drag force acting on the head of the swimmer linearly depends of the velocity and is given by:

$$F_{\text{head}} = -k_{\parallel}(\dot{x} \cdot e_x^h)e_x^h - k_{\perp}(\dot{x} \cdot e_x^h)e_x^h - k_{\perp}(\dot{x} \cdot e_z^h)e_z^h.$$

In matricial form, the force F_{head} can be expressed as:

$$F_{\text{head}} = -R_{\text{head}} \begin{pmatrix} k_{\parallel} & 0 & 0 \\ 0 & k_{\perp} & 0 \\ 0 & 0 & k_{\perp} \end{pmatrix} R_{\text{head}}^T \dot{X}, \tag{2.7}$$

where $k_{\parallel}$ and $k_{\perp}$ are the drag coefficients of the head, and $\dot{X}$ the velocity of the head in the fixed frame.
The torque T_{head} is given by:

$$T_{\text{head}} = -k_r \Omega_{\text{h}}, \tag{2.8}$$

where k_r is the rotational drag coefficient of the head.

Forces and torques on the tail of the swimmer

We consider a point x_i on the i-th link of the tail parametrized by its arclength s such as:

$$x_i(s) = X - rR_{\text{head}}e_x - l\sum_{k=1}^{i-1} R_{\text{head}}R_k e_x - sR_{\text{head}}R_i e_x. \tag{2.9}$$

We differentiate the previous equation to obtain the expression of the velocity $x_i(s)$:

$$\dot{x}_i(s) = \dot{X} - r\dot{R}_{\text{head}}e_x - l\sum_{k=1}^{i-1} \dot{R}_{\text{head}}R_k e_x - l\sum_{k=1}^{i-1} R_{\text{head}}\dot{R}_k e_x - s\dot{R}_{\text{head}}R_i e_x - sR_{\text{head}}\dot{R}_i e_x. \tag{2.10}$$

Following the RFT, the density of the hydrodynamic force $f_i(s)$ acting on the i-th link is linear with respect to the components of $\dot{x}_i(s)$:

$$f_i(s) = -k_{\parallel}(\dot{x}_i(s) \cdot e_x^i)e_x^i - k_{\perp}(\dot{x}_i(s) \cdot e_y^i)e_y^i - k_{\perp}(\dot{x}_i(s) \cdot e_z^i)e_z^i, \tag{2.11}$$

and can be expressed as :

$$f_i(s) = S_i \dot{x}_i(s), \tag{2.12}$$

where

$$S_i = (R_i R_{head}) D (R_{head} R_i)^T, \tag{2.13}$$

with

$$D = - \begin{pmatrix} k_{\parallel} & 0 & 0 \\ 0 & k_{\perp} & 0 \\ 0 & 0 & k_{\perp} \end{pmatrix}. \tag{2.14}$$

Using the expression of $\dot{x}_i(s)$ în the equation (2.11) and angular velocity vectors, the hydrodynamic force density reads as :

$$\begin{aligned} f_i(s) = S_i \dot{X} &- r S_i \Omega_{\mathrm{h}} \times e_x \\ &- l S_i \sum_{k=1}^{i-1} \Omega_{\mathrm{h}} \times R_k e_x \\ &- l S_i \sum_{k=1}^{i-1} R_k \Omega_k \times e_x \\ &- s S_i \Omega_{\mathrm{h}} \times R_i e_x \\ &- s S_i \Omega_{\mathrm{i}} \times e_x. \end{aligned} \tag{2.15}$$

The linear dependency of Ω_{h} in the eq. (2.5)and of Ω_i in 2.6 transform $f_i(s)$ a linear function of $\dot{X}$, $\dot{\Theta}$, and $\dot{\Phi}$:

$$f_i(s) = A_i(s) \begin{pmatrix} \dot{X} \\ \dot{\Theta} \\ \dot{\Phi} \end{pmatrix}, \tag{2.16}$$

where $A_i(s)$ is a $(3, 2N + 6)$ matrix

$$A_i(s) = \begin{pmatrix} A_i^X \in \mathbb{R}^{3\times 3} \\ A_i^{\theta} \in \mathbb{R}^{3\times 3} \\ A_i^1 \in \mathbb{R}^{2\times 3} \\ \vdots \\ A_i^N \in \mathbb{R}^{2\times 3} \end{pmatrix}, \tag{2.17}$$

where

$$A_i(s) = \begin{cases} A_i^X(s) & = S_i, \\ A_i^\theta(s) & = (R_{\text{head}} R_i D R_i^T) \left[r e_x + l \sum_{k=1}^{i-1} R_k e_x \right] L_{\text{h}} + (R_{\text{head}} R_i D R_i^T) \left[s R_i e_x \right] \cdot L_{\text{h}}, \\ A_i^1(s) & = l (R_{\text{head}} R_i D R_i^T) R_1 [e_x] \cdot L_1, \\ & \vdots \\ A_i^{i-1}(s) & = l (R_{\text{head}} R_i D R_i^T) R_{i-1} [e_x] \cdot L_{i-1}, \\ A_i^i(s) & = s (R_{\text{head}} R_i D) [e_x] \cdot L_i, \\ A_i^j(s) & = 0_3 \quad \forall j > i. \end{cases} \tag{2.18}$$

We define the two $3 \times (2N+6)$ matrices B^i and C^i as :

$$\begin{cases} B_i = \int_0^l A_i(s)\, ds, \\ C_i = \int_0^l s A_i(s)\, ds. \end{cases} \tag{2.19}$$

The hydrodynamic force on link i depends linearly on the $\dot{X}, \dot{\Theta}, \dot{\Phi}$ as follows:

$$F_i = B_i \begin{pmatrix} \dot{X} \\ \dot{\Theta} \\ \dot{\Phi} \end{pmatrix}. \tag{2.20}$$

The hydrodynamic torque on link i compute from he head center as follows:

$$T_i = \int_0^l (x_i(s) - X) \times f_i(s)\, ds. \tag{2.36}$$

By using equation (2.9), we obtain

$$T_i = - \left[r R_{\text{head}} e_x + \sum_{k=1}^{i-1} l R_{\text{head}} R_k e_x \right] \times \int_0^l f_i(s)\, ds - [R_{\text{head}} R_i] \times \int_0^l s f_i(s)\, ds, \tag{2.21}$$

which depends linearly on the $\dot{X}, \dot{\Theta}, \dot{\Phi}$ as follows:

$$T_i = - \left(\left[r R_{\text{head}} e_x + \sum_{k=1}^{i-1} l R_{\text{head}} R_k e_x \right] \times B_i \right) \begin{pmatrix} \dot{X} \\ \dot{\Theta} \\ \dot{\Phi} \end{pmatrix} - ([R_{\text{head}} R_i] \times C_i) \begin{pmatrix} \dot{X} \\ \dot{\Theta} \\ \dot{\Phi} \end{pmatrix}. \tag{2.22}$$

2.3.2 Equation of Motion

The equation of motion of the swimmer, which relies on self-propulsion, is given by the balance of forces and torques applied to the head and the links, assuming no external forces or torques are present as:

$$\begin{cases} F_h + \sum_{i=1}^{N} F_i = 0, \\ T_h + \sum_{i=1}^{N} T_i = 0. \end{cases} \tag{2.23}$$

The previous system can be rewritten matricially as :

$$M(\Theta, \Phi) \begin{pmatrix} \dot{X} \\ \dot{\Theta} \\ \dot{\Phi} \end{pmatrix} = 0, \tag{2.24}$$

with M a matrix of dimension $6 \times (2N+6)$. The matrix $M(\Theta, \Phi) \in \mathbb{R}^{6\times(2N+6)}$ can be subdivided into two sub-matrices $M_{X,\Theta}(\Theta, \Phi) \in \mathbb{R}^{6\times 6}$ and $M_{\Phi}(\Theta, \Phi) \in \mathbb{R}^{6\times 2N}$ such that

$$M(\Theta, \Phi) = \left(M_{X,\Theta}(\Theta, \Phi) \mid N_{\Phi}(\Theta, \Phi)\right). \tag{2.25}$$

Using these sub-matrices in equation (2.24), and assuming that the values of $\dot{\Phi}(t)$ are prescribed, the position and orientation of a self-propelled swimmer can be obtained from the deformations of its tail by solving the following differential system:

$$\begin{pmatrix} \dot{X} \\ \dot{\Theta} \end{pmatrix} = M_{X,\Theta}^{-1}(\Theta, \Phi) N_{\Phi}(\Theta, \Phi)\dot{\Phi}. \tag{2.26}$$

To sumarize the modelisation of the swimmer :

- The swimmer is described by 2N+6 variables; 6 positions variables and 2N shape variables.
- The position variables are X, the Cartesian coordinates of the swimmer's head, and $\Theta = (\theta_x^i, \theta_y^i, \theta_z^i)$, its orientation.
- The shape variables are the angles ϕ_y^i and ϕ_z^i of the i-th segment.
- The dynamics of the swimmer can be described by a linear control system where the control $u(t)$ represents the derivatives of Φ

$$\begin{pmatrix} \dot{\Phi} \\ \dot{X} \\ \dot{\theta} \end{pmatrix} = \tilde{M}_{X,\Theta}^{-1}(\Theta, \Phi)\tilde{M}_{\Phi}(\Theta, \Phi)u(t) \tag{2.27}$$

Chapter 3

Numerical Results

In this chapter, we test the validity of the model by comparing the displacement of the swimmer, as well as the translational and angular velocities, with experimental results from the literature. To do this, we prescribe a deformation velocity to the flagellum in our model, associated with planar displacement [4] and non-planar displacement [7]. We then study the influence of the different parameters constituting the N-links model to understand their role in the swimmer's displacement.

3.1 Planar Displacement of the swimmer

3.1.1 The deformation of the tail over the time

For sperm cells swimming close to a planar boundary surface, nearly planar beat patterns were observed, with the flagellar beating approximately parallel to the boundary surface. as show in Figure 3.1. The position of the vector $r(s,t)$ can be expressed in the head frame with $e_1(t)$ as unit vector parallel to the long axis of the sperm head and $e_2(t)$, which is obtained by rotating e_1 in the swimming plane by an angle of $\pi/2$ in a counter-clockwise. The shape of the flagellar centreline $r(s,t)$ at time t is characterized by a tangent angle $\psi(s,t)$ for all arc length position s, with s in the range $[0, L]$, L be the length of the flagellum.

The expression of $r(s,t)$ can be expressed as

$$r(s,t) = \frac{L_{\text{head}}}{2} e_1(t) + \int_0^s \left[\cos(\psi(u,t))e_1(t) + \sin(\psi(u,t))e_2(t)\right] du, \quad [4] \tag{3.1}$$

where $\psi(s,t)$ expression is given by:

$$\psi(s,t) = K_0 s + 2A_0 s \cos(\omega t - \frac{2\pi s}{\lambda}).$$

with λ the wavelength of the flagellar wave, ω the angular frequency of the flagellar beat ,K_0 a simple measure for the asymmetry of the mean shape of the flagellum and A_0 the amplitude of curvature.

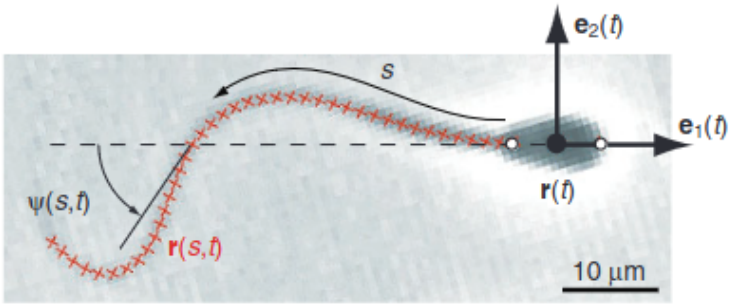

Figure 3.1: Description of the parametrisation of the head and the tail of the swimmer. The position of the head center is defined by $r(t)$, the origin of the head frame$(e_1(t), e_2(t))$. The position of the tail is described by $r(s,t)$, the image is taken from [4]

The setup we used to simulate the motion of the tail of the swimmer is presented in Table 3.1

Parameter	Value	Description
N	15	Number of points from the flagellum discretization
A_0	$15.2 \times 10^3\,\mathrm{rad/m}$	Initial Amplitude
ω_0	$(2\pi/23) \times 10^3$	Angular frequency
λ	$(2\pi/29.6) \times 10^6$	Wavelength
L	λ	Length of the flagellum
t_{vals}	$\left\{0, \ldots, \frac{2\pi}{\omega}\right\}$	Time over one period
NT	100	Number of points time discretisation
K_0	$35.1 \times 10^3\,\mathrm{N/m}$	Stiffness constant
B	$160 \times 10^3\,\mathrm{N \cdot m^2}$	Bending modulus
A_0	$15.2 \times 10^3\,\mathrm{rad/m}$	Initial amplitude
r	$2.5 \times 10^{-6}\,\mathrm{m}$	Radius
τ_f	$0.00477\,\mathrm{mm}^{-1}$	Twist
ν	$0.7 \times 10^9\,\mathrm{Ns/m^2}$	Viscosity
$k_{k,\mathrm{tail}}$	$0.99 \times \nu$	Parallel friction (tail)
$k_{\perp,\mathrm{tail}}$	$1.81 \times k_{k,\mathrm{tail}}$	Perpendicular friction (tail)
$k_{\perp,\mathrm{head}}$	$46.1 \times 10^3\,\mathrm{N}$	Perpendicular friction (head)
$k_{k,\mathrm{head}}$	$40.3 \times 10^3\,\mathrm{N}$	Parallel friction (head)
k_r	$0.84 \times 10^{-6}\,\mathrm{N}$	Rotational friction
T_{final}	$\frac{2\pi}{\omega} \times 40$	Time of simulation

Table 3.1: Parameters used in the simulation

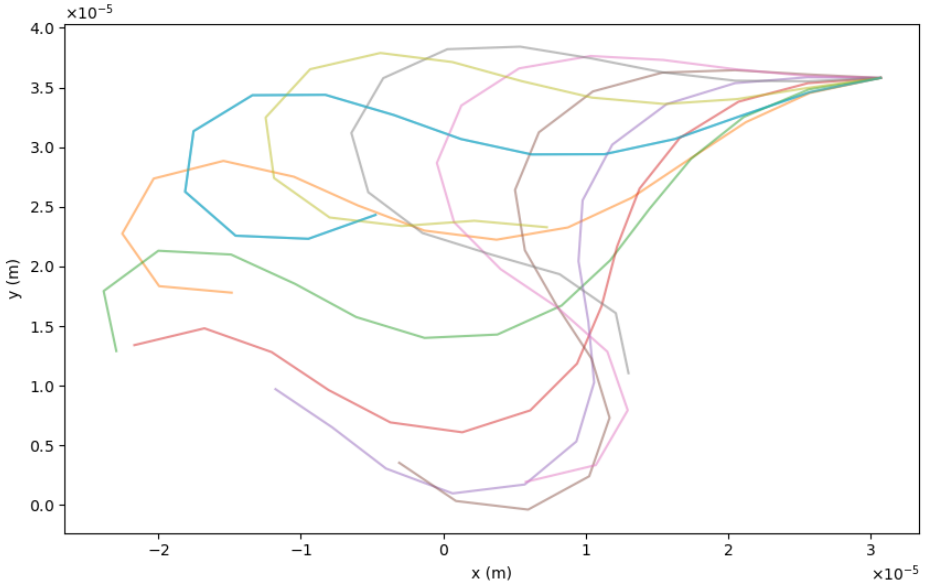

Figure 3.2: The position of the tail according the parameters in Table 3.1

The Figure 3.2 illustrates the displacement of a flagellum over time. The flagellum oscillates periodically, which facilitates the movement of the micro-swimmer. Each colored curve represents the position of the flagellum at different moments in beat cycle.

3.1.2 The displacement of the head over the time

We solve (2.26) to obtain the position of the head of the swimmer over the time. The results we obtain are similar to those presented in the article [4] and [5]

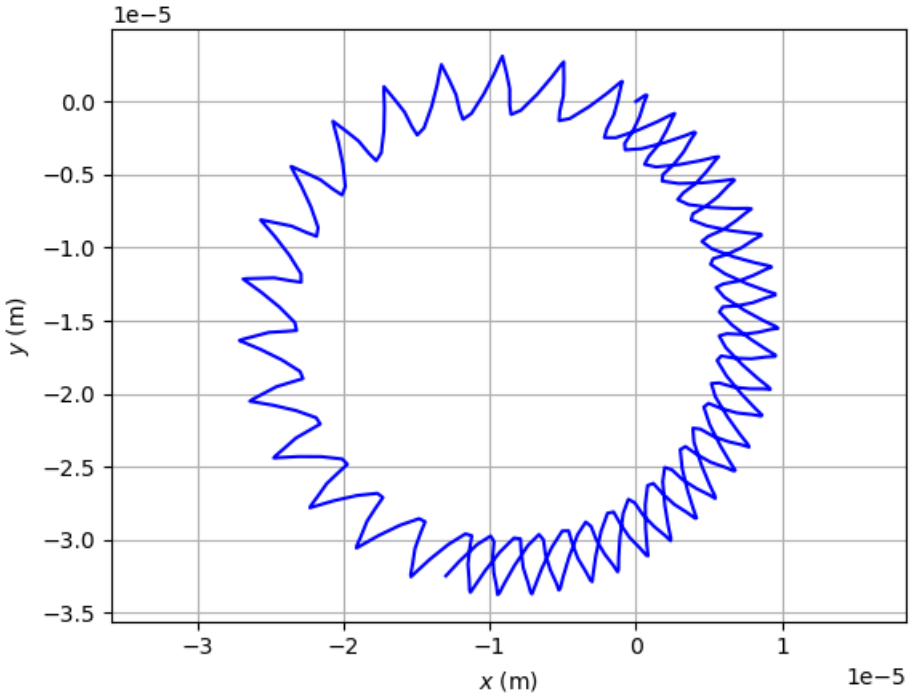

Figure 3.3: The motion of the head of the swimmer in the frame (e_x, e_y) with the flagellum beat (3.1), using the parameters in Table 3.1

We compute also the parrallel, orthogonal and rotational velocity of of the swimmer head and obtain results which are similary at [4]

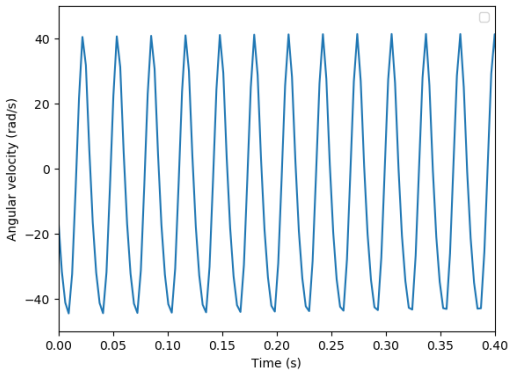

(a)

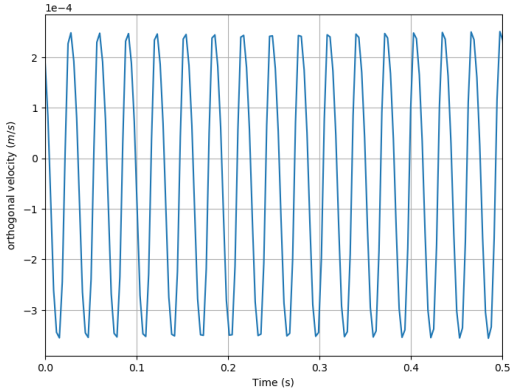

(b)

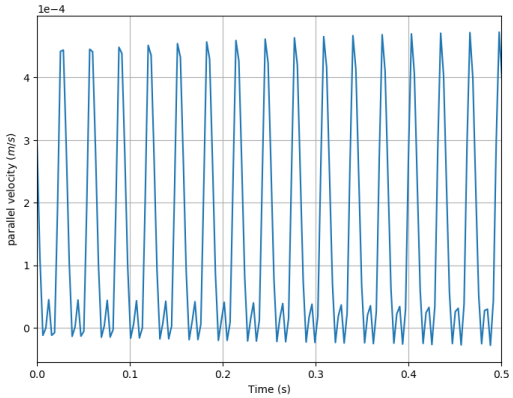

(c)

Figure 3.4: (a) Angular velocity of the swimmer head, (b) orthogonal velocity of the swimmer head and (c) parallel velocity of the swimmer head.

In order to study the influence of the differents parameters that characterize the swimmer, We varied the number of discretization points and the

drag coefficient of the head; here are some of the results we obtained

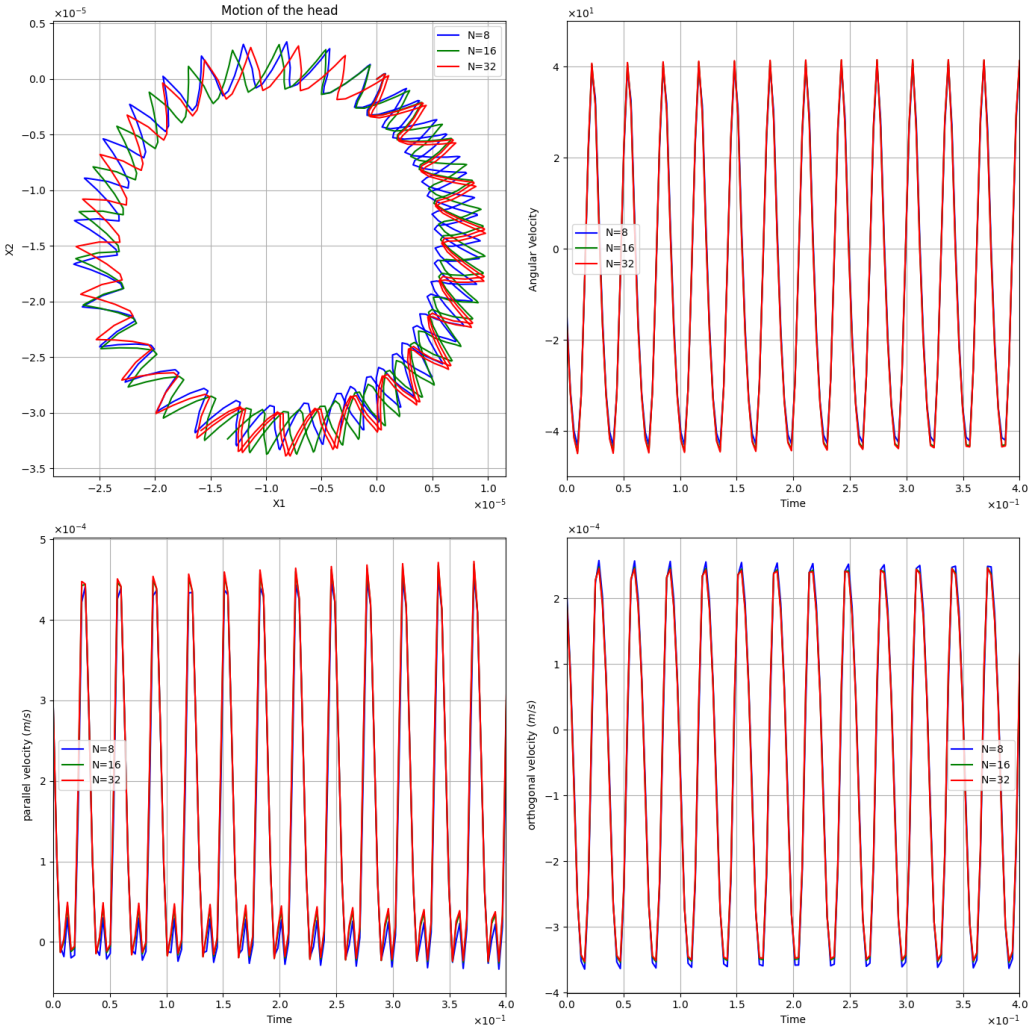

Figure 3.5: Comparison of head motion and translational velocities based on the number of discretization points N using the parameters in Table 3.1. (Top left) Motion of the head in the (x, y) plane, (Top right) Angular velocity of the head over time, (Bottom left) Translational velocity of the head along the x axis, (Bottom right) Translational velocity of the head along the y axis.

By increasing the number of links, the discretization becomes finer, which improves the accuracy of the model in simulating head motion. This is particularly visible in the oscillations of trajectory and velocity, which become more regular and in line with theoretical expectations.

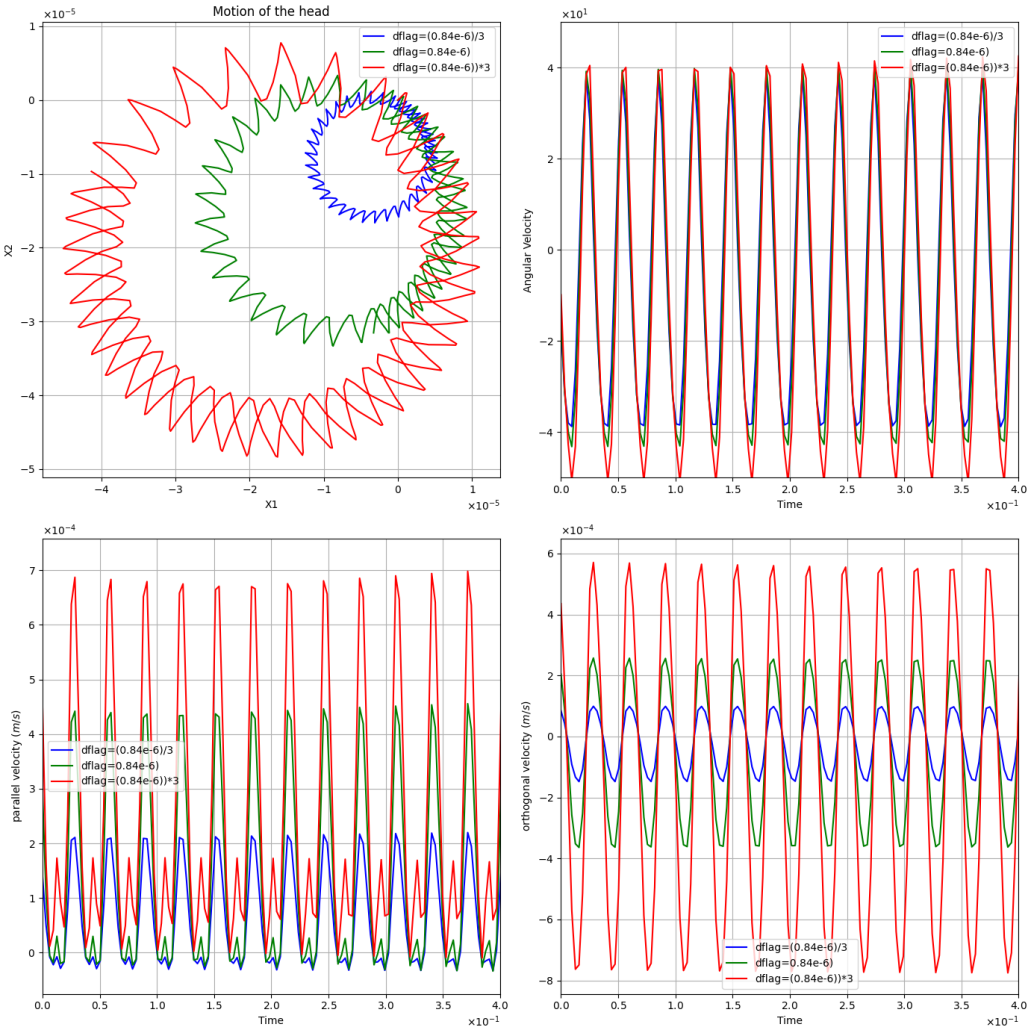

Figure 3.6: Modification of the parallel drag coefficients of the flagellum while keeping the head's drag coefficients and the value of N constant. (Top left) Motion of the head in the (x, y) plane for different drag coefficients on the tail, (Top right) Angular velocity of the head over time for different drag coefficients, (Bottom left) Translational velocity of the head along the x axis over time, (Bottom right) Translational velocity of the head along the y axis over time.

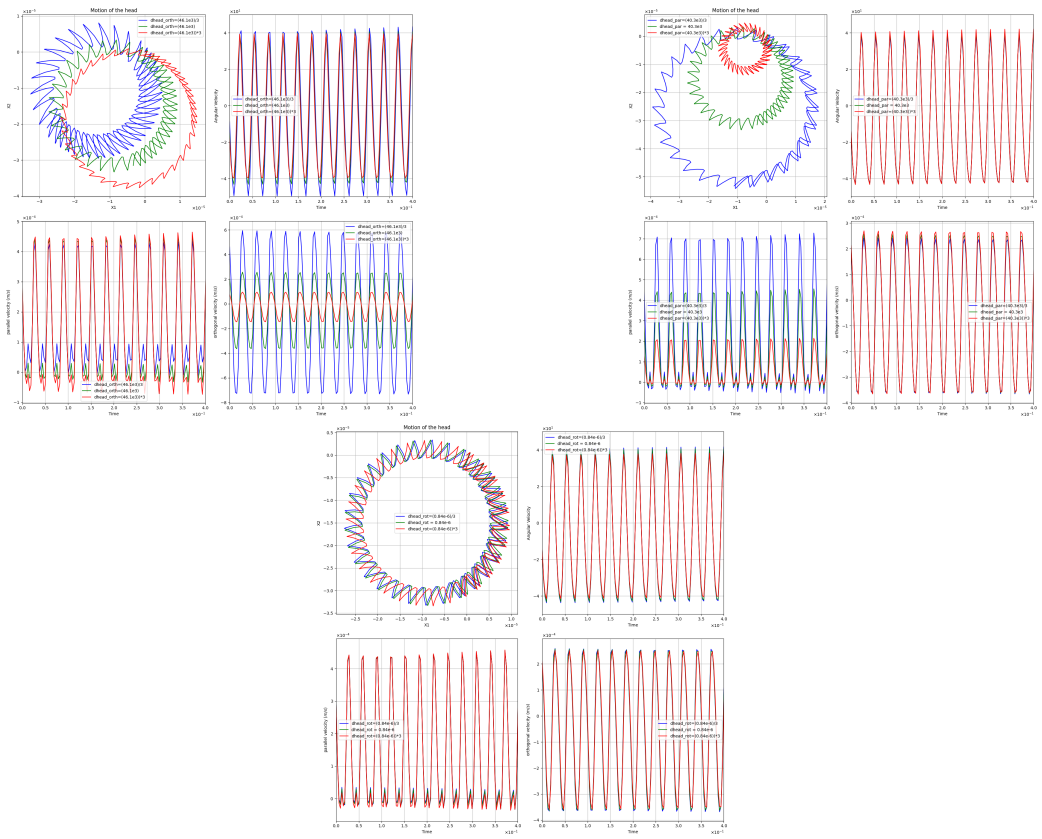

Figure 3.7: (top left) Modification of the rotational friction while keeping the head's drag coefficients and the value of N constant, (top right) Modification of the parallel friction of the head while others drag coefficients and the value of N constant, (bottom left) Modification of the orthogonal friction of the head while others drag coefficients and the value of N constant using the parameters in Table 3.1

Drag coefficients have a decisive influence on the movement of a flagellum in a fluid. They modify the resistance encountered by the flagellum as it moves, directly affecting the shape and size of its trajectory. More specifically, parallel and perpendicular drag coefficients play an essential role in determining the circular motion of a micro-swimmer's head.

When these coefficients are high, they increase the drag force, which can lead to a widening of the radius of the flagellum's circular motion. Conversely, lower drag coefficients reduce this force, thus tightening the curvature of the trajectory.

3.2 Non planar displacement of the swimmer

3.2.1 The deformation of the tail over the time

We present the results obtained in the case of non planar motion of the tail and the head. What differentiates the non planar movement from the the planar case is the way we compute the derivatives $\dot{\phi}^i$ of the links. it is same ODE system we use to resolve the position of the swimmer's head over time in the non planar movement. The article we used to validate our results is [7] The equation of the motion of the flagellum is expressed by:

$$\begin{cases} \frac{d\mathbf{r}(\mathbf{s},\mathbf{t})}{ds} & = \psi_1(s,t), \\ \frac{d\psi_1(s,t)}{ds} & = k_f\psi_3(s,t), \\ \frac{d\psi_2(s,t)}{ds} & = \tau_f\psi_3(s,t), \\ \frac{d\psi_3(s,t)}{ds} & = -k_f\psi_1(s,t) + \tau_f\psi_2(s,t). \end{cases} \tag{3.2}$$

with $\psi_i \in \mathbb{R}^3$, $i \in \{1,2,3\}$, k_f and τ_f are the flagellar curvature and twist, respectively. We assume a constant flagellar twist τ_f and a flagellar curvature k_f given by a travelling bending wave,

$$k_f(l,t) = K_0 + B\cos(\omega_0 t - \lambda l), \tag{3.3}$$

where K_0 is the mean curvature, B the amplitude, ω_0 the angular frequency, and λ the wavelength, which are defined in Table 3.1. We can rewrite the equation (3.1) in the matricial form as:

$$\frac{d}{ds}\begin{pmatrix} \mathbf{r} \\ \psi_1 \\ \psi_2 \\ \psi_3 \end{pmatrix} = A(s,t)\begin{pmatrix} \mathbf{r} \\ \psi_1 \\ \psi_2 \\ \psi_3 \end{pmatrix} \tag{3.4}$$

with

$$A(s,t) = \begin{pmatrix} 0 & 1 & 0 & 0 \\ 0 & 0 & 0 & k_f \\ 0 & 0 & 0 & -\tau_f \\ 0 & -k_f & \tau_f & 0 \end{pmatrix}.$$

The resolution of (3.4) for each t provides us with the position of the swimmer's tail over time, as well as ψ, and then the derivatives Φ

$$\phi_y^i = \arctan\left(\frac{(\psi_1(0^i,t))_2}{(\psi_1(O^i,t))_1}\right), \tag{3.5}$$

$$\phi_z^i = \arctan\left(\frac{(\psi_3(O^i,t))_2}{(\psi_3(O^i,t))_1}\right), \tag{3.6}$$

where O^i is the i-point of the discretized flagellum

The angular derivative is approximated by a central finite difference. We consider Δt to be the time step size defined as $\frac{T_{\text{final}}}{NT-1}$, where T_{final} is the total simulation time.

$$\dot{\phi}_j(t) = \frac{\phi_j(t+\Delta t) - \phi_j(t-\Delta t)}{2\Delta t} + O(\Delta t^2),$$

and for $t = 0$, we have:

$$\dot{\phi}_j(0) = \frac{\phi_j(\Delta t) - \phi_j(-\Delta t)}{2\Delta t}.$$

The problem arises when we want to calculate the angular velocity at $t = 0$, because we don't have the value of $\phi_j(-\Delta t)$. For this, we discretized the time such that we add $-\Delta t$ and $T_{\text{final}} + \Delta t$ to the time vector in order to use the finite difference method

We was able to have the results of the deformation of the tail which are similary to those presented in this article [7]

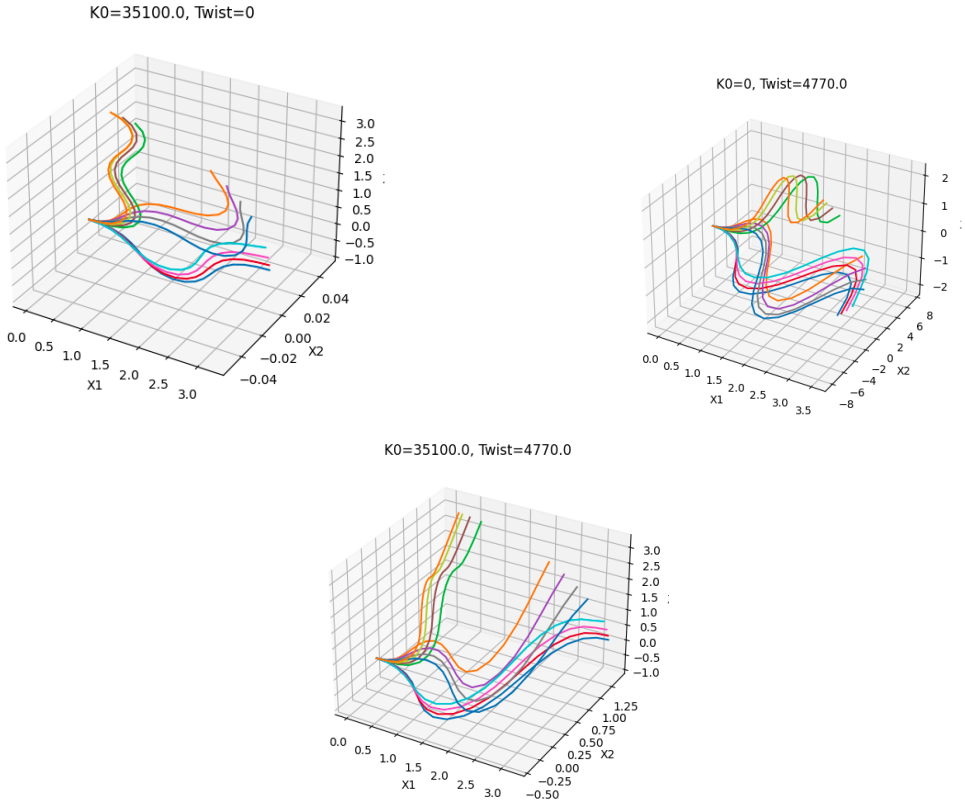

Figure 3.8: Motion of the tail for three test case for N = 10. Top left ($K_0 = 35100$, Twist = 0): The trajectory is smooth and controlled by the stiffness K_0, with no influence from the twist. This results in a regular and predictable movement. Top right ($K_0 = 0$, Twist = 4770.0): In the absence of stiffness, the high twist ($Twist = 4770.0$) leads to a more complex and varied trajectory. Bottom ($K_0 = 35100$, Twist = 4770.0): This case combines both stiffness and twist, resulting in a trajectory that displays characteristics of both smoothness and complexity, reflecting the combined influence of these two parameters.

3.2.2 The displacement of the Head over the time

We present here the results, obtained in the non planar frame of the head motion which are similary to the ones presented in [7]

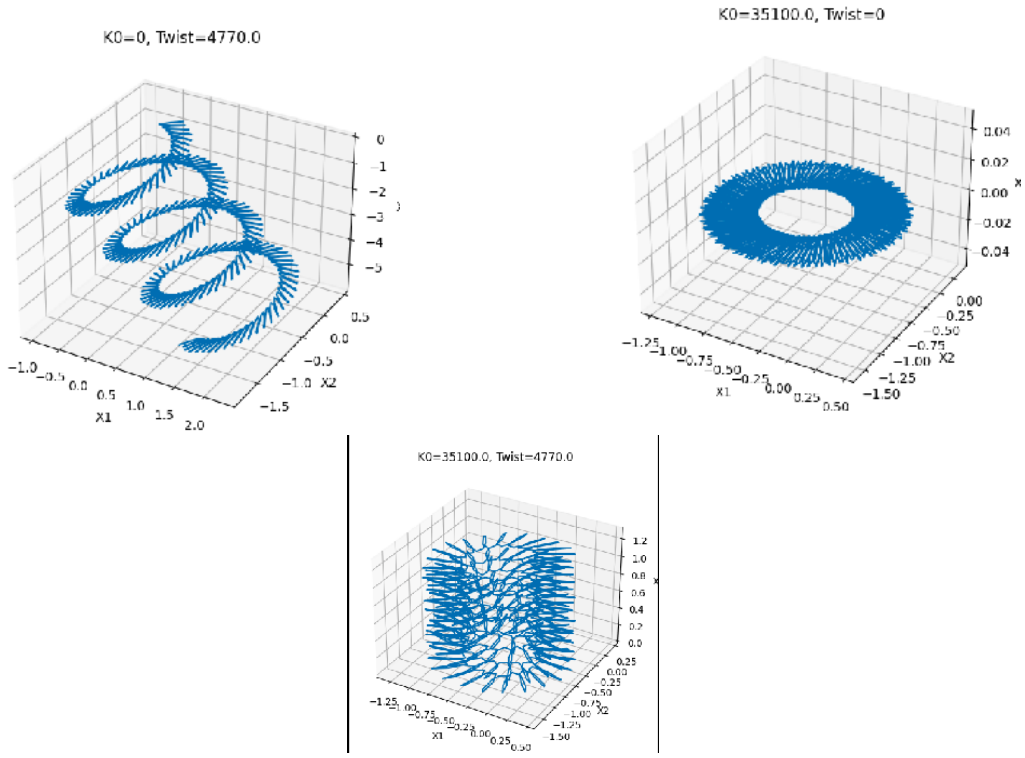

Figure 3.9: Motion of the Head for three test case for NT = 1000. Top Left ($K_0 = 0$, Twist = 4770.0): The trajectory is helical, indicating that the high twist value fully dictates the motion in the absence of stiffness ($K_0 = 0$). The lack of resistance to bending allows the twist to create a pronounced spiral path. Top Right ($K_0 = 35100$, Twist = 0): The motion is circular and stable, driven primarily by the stiffness K_0. The absence of twist results in a smooth and predictable trajectory. Bottom ($K_0 = 35100$, Twist = 4770.0): The trajectory is dense and complex, reflecting the combined effects of both stiffness and twist.

3.3 Conclusion

In the chapter 2, we presented a dynamic model that represents the motion of a micro-swimmer equipped with a flagellum. This model, designed to be easy to implement and solve, is well-suited for predicting the behavior of microorganisms in low Reynolds number environments.

In this chapter our goal was to apply this model and simulate the micro-swimmer's motion both in planar and non-planar reference frames. The results we obtained closely align with those found in the literature, particularly in the studies by [4, 7]. This consistency with existing research demonstrates

the model's accuracy and reliability. Moreover, the model proves to be a valuable tool for the subsequent analysis of optimal control strategies for the swimmer's trajectory, which we will address in the next section.

Chapter 4

Optimal control

4.1 Introduction

Control theory deals with systems that can be controlled i.e whose evolution can be influenced. The goal is to bring a system from a given initial state to a certain final state while respecting the constraints applied to the system. A control system is said to be controllable if it can be brought (in finite time) from an arbitrary initial state to a prescribed final state. Once a controllability is assured, one might also want to reach the final state while minimizing a cost criterion; this is known as an optimal control problem.

The problem considered in this Chapter is as follows: Let $(n, m) \in \mathbb{N}^*$, I be an interval of $\mathbb{R}$, and f a function from $\mathbb{R}_+ \times \mathbb{R}^n \times \mathbb{R}^m$ to $\mathbb{R}^n$ chosen to be sufficiently regular. Let U be a subset of $\mathbb{R}^m$ and let $x_0 \in \mathbb{R}^n$. The linear control system of interest is:

$$\begin{cases} \dot{x}(t) = f(t, x(t), u(t)) \quad \forall t \in I \\ x(0) = x_0. \end{cases} \tag{4.1}$$

where the set of controls u considered is the set of measurable and bounded functions on I, taking values in the subset U. Assuming that the system is controllable, it is defined by:

$$\begin{cases} \inf\limits_{u \in U_{\text{ad}}} C(u, t) = g(x(T), T) + \int_0^T f(x(t), u(t))\, dt, \\ \dot{x}(t) = f(t, x, u) \\ x(0) = x_0. \end{cases} \tag{4.2}$$

wth U_{ad} represents the set of all admissible controls that can be applied to a system.
We focused on two types of problems (4.5)and (4.6) to understand the control

optimal to understand optimal control, and once understood, the goal is to apply it to the N-link model.

4.2 Optimal control of a train

We study the rectilinear motion of a train following a given trajectory while controlling its acceleration, meaning

$$\begin{cases} \dot{x} = y, \\ y = u. \end{cases} \tag{4.3}$$

First, we maximize the distance traveled by the train starting from the origin while considering the energy expended. We focus on the final time T to assess the maximum distance:

$$\inf C(u,T) = \underbrace{-x(T)}_{\text{distance}} + \underbrace{\int_0^T \|u(t)\|_2^2 \, dt}_{\text{energy expended}} \tag{4.4}$$

with

$$\begin{cases} u \in U_{\text{ad}} \text{ where } U_{\text{ad}} = \{u \in L^2([0,T],\mathbb{R})\} \\ \dot{x}(t) = y(t) \\ y(t) = u(t) \quad \forall t \in [0,T] \\ x(0) = x_0 = 0 \\ y(0) = y_0 = 0. \end{cases} \tag{4.5}$$

We can demonstrate the existence and uniqueness of the problem, and the exact solution associated with this problem is of the form:

$$u(t) = \frac{T-t}{2}.$$

Second, we address the problem of returning the train to a station in minimal time while avoiding a crash (i.e., ensuring zero velocity upon arrival), we impose a constraint on the control by bounding it. The associated system is as follows:

$$\inf C(u,T) = T \tag{4.6}$$

$$\begin{cases} u \in U_{\text{ad}} \text{ where } U_{\text{ad}} = \{u \in L^2([0,T],\mathbb{R}) \\ \qquad\qquad\qquad \text{such that } |u(t)| \leq 1 \quad \forall t \in [0,T]\} \\ \dot{x}(t) = y(t) \\ y(t) = u(t) \quad \forall t \in [0,T] \\ x(0) = x_0 \neq 0 \\ y(0) = y_0 \neq 0 \\ x(T) = 0 \\ y(T) = 0. \end{cases} \tag{4.7}$$

The exact solution to this problem is of the bang-bang type. A bang-bang control refers to a control strategy where the control input $u(t)$ switches abruptly between its extreme values in this case, between -1 and 1.

To solve these two problems, we used CasADi [3], an open-source tool for nonlinear optimization and algorithmic differentiation, we use multiple shooting [12] numerical methods which we are going present to next in the section.

4.3 Numerical Method : Multiple shooting

The multiple shooting method is an advanced numerical technique used to solve optimal control problems. It divides the total time interval $[0, T]$ into several sub-intervals. For each sub-interval, decision variables u_k for control and x_k for the system state are assigned. Unlike a continuous state function $x(t)$, this method uses discrete variables $x_1, x_2, \ldots, x_{N+1}$ that represent the states at the boundaries of each sub-interval.

For each sub-interval, a numerical integration of the ordinary differential equation (ODE) is performed. For instance, using explicit Euler, an approximation of the form $x_{k+1} \approx x_k + \frac{T}{N} f(x_k, u_k)$ is obtained, or more generally $x_{k+1} = F(x_k, u_k)$. The integrator predicts where the system will be at the end of each sub-interval, allowing the controls to be adjusted to optimize the overall trajectory while respecting continuity constraints between sub-intervals.

This method is particularly useful for handling complex initial and final conditions, as well as constraints on the system's state and controls, enabling a more robust and precise solution to optimal control problems.

The results we obtained by applying this numerical method to our two problems are as follows :

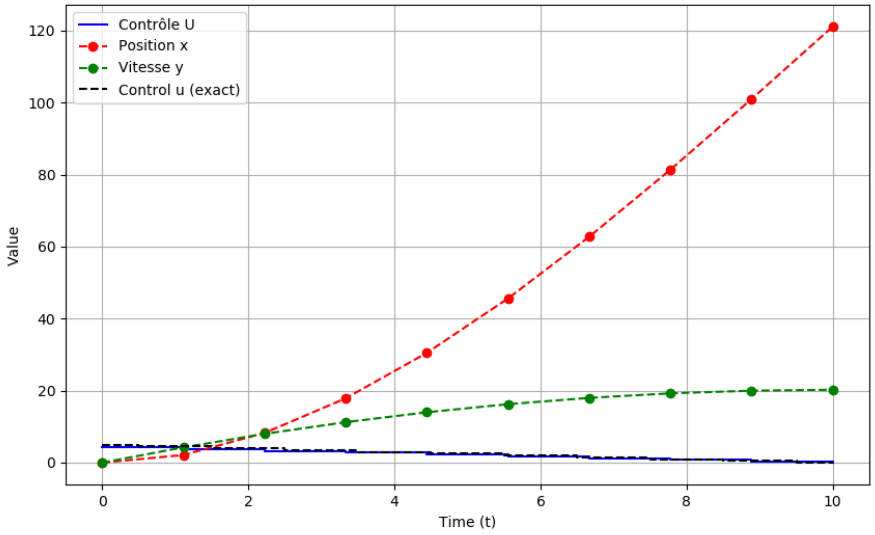

Figure 4.1: This figure shows that a low and nearly constant control (blue line) helps minimize energy while steadily increasing the train's position (red line) and stabilizing its velocity (green line). The exact control (black dashed line) closely matches the calculated control, meaning the initial control is nearly optimal for energy efficiency for the problem (4.5)

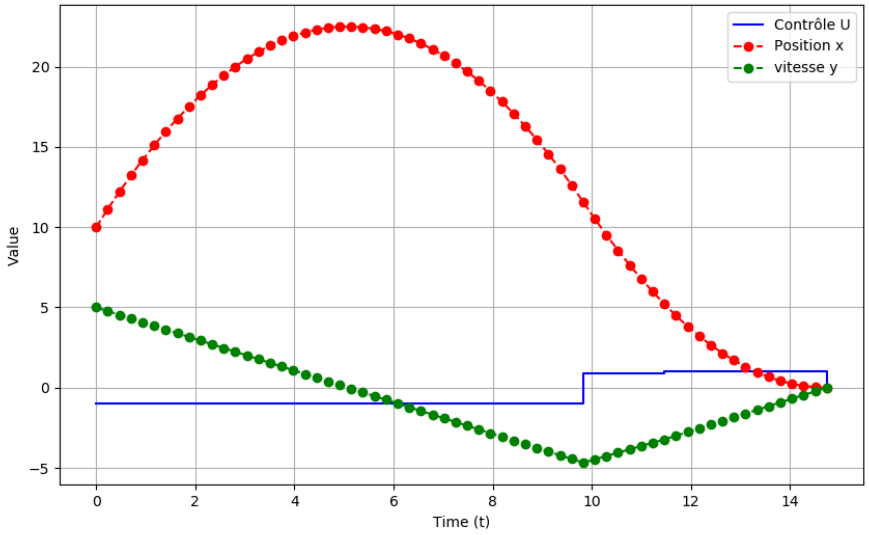

Figure 4.2: Solution to Problem (4.6): this figure shows a bang-bang control where $u(t)$ (blue line) switches from 1 to -1. This control first accelerates the system (position $x(t)$ increases, red line), then decelerates it (position decreases, velocity $y(t)$ stabilizes, green line), to reach the final state with zero velocity.

4.4 Optimal Control of the N-link swimmer

The optimal control of N-link micro-swimmers is a crucial area of study for understanding and manipulating the movements of these systems in fluid environments with low Reynolds numbers. In the article "Controllability and Optimal Strokes for N-link Micro-swimmer," [5], they explore the principles of controllability of these micro-swimmers and develop optimal movement strategies ("strokes") that allow achieving specific objectives, such as displacement or orientation in a fluid, while minimizing the energy consumed or the time required. This study highlights the possibility of fully controlling the position and orientation of the micro-swimmer. The equation associated with the problem is:

$$c(u,T) = -x(T) + \int_0^T \|u(t)\|^2 \, dt$$

where $x(T)$ represents the final state that we wish to maximize (such as the final position or orientation), and $\|u(t)\|^2$ represents the energy or control

effort that we seek to minimize over time.

However, due to a lack of time, we were unable to implement this solution fully.

Chapter 5

Conclusion

During my internship, we focused on understanding and validating a previously developed, accurate and computationally efficient dynamic model for a three-dimensional flagellated micro-swimmer. This model has demonstrated its effectiveness in predicting the displacements of low-Reynolds number swimmers, But it has also been validated through comparisons with the results of the articles we have used. While the primary focus of this study has been on the general modeling of micro-swimmers, the model also serves as a robust foundation for investigating the locomotion of biological flagellated micro-swimmers.

The model utilizes a Resistive Force Theory-based approximation for hydrodynamics, along with a discrete shape approximation for the swimmer's tail geometry. This approach results in an ordinary differential equation (ODE) modeling the motion of mono-flagellated swimmer. On top of that, this formulation allows the dynamics of the swimmer to be represented as an affine ODE control system, making it particularly suitable as a dynamic constraint in optimal control problems

The next challenge is to study some optimal control on the swimmer by using multiple shooting method. Unfortunately, we were unable to obtain results within the available time, but we have developed an algorithm with this objective in mind.

Bibliography

[1] Jake J. Abbott, Kathrin E. Peyer, Marco Cosentino Lagomarsino, Li Zhang, Lixin Dong, Ioannis K. Kaliakatsos, and Bradley J. Nelson. How should microrobots swim? *The International Journal of Robotics Research*, 28(11-12):1434–1447, 2009. (Cited on pages iii, 5 and 44).

[2] Yacine El Alaoui-Faris. *Modélisation et contrôle optimal de micro-nageurs magnétiques*. PhD thesis, Université Côte d'Azur, 2022. (Cited on pages 20, 23 and 24).

[3] J. Andersson, J. Gillis, G. Horn, J. Åkesson, and M. Diehl. Casadi: a software framework for nonlinear optimization and optimal control. `https://web.casadi.org/docs/`, 2023. Accessed: 2023-10-04.

[4] B. M. Friedrich, I. H. Riedel-Kruse, J. Howard, and F. Jülicher. High-precision tracking of sperm swimming fine structure provides strong test of resistive force theory. *Journal of Experimental Biology*, 213(8):1226–1234, Apr 2010.

[5] L. Giraldi, P. Martinon, and M. Zoppello. Controllability and optimal strokes for n-link microswimmer. In *52nd IEEE Conference on Decision and Control*, pages 3870–3875, Firenze, Dec 2013. IEEE.

[6] J. Gray and G. J. Hancock. The propulsion of sea-urchin spermatozoa. *Journal of Experimental Biology*, 32(4):802–814, Dec 1955.

[7] J. F. Jikeli, L. Alvarez, B. M. Friedrich, L. G. Wilson, R. Pascal, R. Colin, M. Pichlo, A. Rennhack, C. Brenker, and U. B. Kaupp. Sperm navigation along helical paths in 3d chemoattractant landscapes. *Nature Communications*, 6(1):7985, Aug 2015.

[8] Clement Moreau, Laetitia Giraldi, and Hermes Augusto Buarque Gadelha. The asymptotic coarse-graining formulation of slender-rods, bio-filaments and flagella. *Journal of the Royal Society Interface*, 2018. (Cited on pages 20, 23 and 24).

[9] Constantine Pozrikidis and D. Jankowski. *Introduction to Theoretical and Computational Fluid Dynamics*, volume 675. Oxford University Press, New York, 1997. (Cited on pages 2 and 3).

[10] E. M. Purcell. Life at low reynolds number. *American Journal of Physics*, 45(1):3–11, Jan 1977.

[11] G. Taylor. Analysis of the swimming of microscopic organisms. *Proceedings of the Royal Society of London A*, 209:447–461, 1951.

[12] Emmanuel Trélat. Contrôle optimal: Théorie et applications. `https://www.ljll.fr/~trelat/fichiers/livreopt.pdf`, 2023. Accessed: 2023-10-04, page 194.